## Title
Vascular Remodeling in Autogenous Arterio-Venous Fistulas by MRI and CFD



## Journal
Annals of Biomedical Engineering, 41(4)

## ISSN
0145-3068

## Authors
Sigovan, Monica
Rayz, Vitaliy
Gasper, Warren
et al.

## Publication Date
2013-04-01

## DOI
10.1007/s10439-012-0703-4

Peer reviewed

Published in final edited form as:
*Ann Biomed Eng*. 2013 April ; 41(4): 657–668. doi:10.1007/s10439-012-0703-4.

# Vascular Remodeling in Autogenous Arterio-Venous Fistulas by MRI and CFD

**Monica Sigovan**[1], **Vitaliy Rayz**[1], **Warren Gasper**[2], **Hugh F. Alley**[2], **Christopher D. Owens**[2,3], and **David Saloner**[1,4]

[1]Department of Radiology and Biomedical Imaging, University of California, San Francisco, 4150 Clement Street, Box 411D, San Francisco 94121, CA, USA

[2]Department of Vascular Surgery, University of California, San Francisco, CA, USA

[3]Vascular Surgery Service, VA Medical Center, San Francisco, CA, USA

[4]Radiology Service, VA Medical Center, San Francisco, CA, USA

## Abstract

Hemodynamic parameters play an important role in regulating vascular remodeling in arterio-venous fistula (AVF) maturation. Investigating the changes in hemodynamic parameters during AVF maturation is expected to improve our understanding of fistula failure, but very little data on actual temporal changes in human AVFs is available. The present study aimed to assess the feasibility of using a noncontrast-enhanced MRI protocol combined with CFD modeling to relate hemodynamic changes to vascular remodeling following native AVF placement. MR angiography (MRA) and MR velocimetry (MRV) data was acquired peri-operatively, 1 month, and 3 months later in three patients. Vascular geometries were obtained by segmentation of the MRA images. Pulsatile flow simulations were performed in the patient specific vascular geometries with time-dependent boundary conditions prescribed from MRV measurements. A principal result of the study is the description of WSS changes over time in the same patients. The disturbed flow observed in the venous segments resulted in a variability of the WSS distribution and could be responsible for the non-uniform remodeling of the vessel. The artery did not show regions of disturbed flow upstream from the anastomosis, which would be consistent with the uniform remodeling. MRI use demonstrated the ability to provide a comprehensive evaluation of clinically relevant information for the investigation of upper extremity AVFs. 3D geometry from MRA in combination with MRV provides the opportunity to perform detailed CFD analysis of local hemodynamics in order to determine flow descriptors affecting fistula maturation.

### Keywords

Computational fluid dynamics; Magnetic resonance imaging; Vascular access; Hemodialysis fistula; Vascular remodeling; WSS

## INTRODUCTION

The incidence of kidney failure has increased dramatically due to the increasing prevalence of diabetes and an increase in the aging population. These patients require permanent vascular access for dialysis therapy. Although native arterio-venous fistulas (AVF) are



Address correspondence to Monica Sigovan, Department of Radiology and Biomedical Imaging, University of California, San Francisco, 4150 Clement Street, Box 411D, San Francisco 94121, CA, USA. monica.sigovan1@gmail.com.

recommended and widely used, given their superiority to grafts,[13] they are very prone to complications during maturation, with a high incidence of primary failure (or a failure to mature).[6,23,30] AVF maturation is an active process of vascular remodeling that is a response to the altered biomechanical forces induced in the vascular system by placement of the fistula. At the time of fistula placement, the venous segment is transposed into the arterial circulation following which the vessel remodels adjusting to the increased flow and pressure. Complications, such as impaired remodeling, stenosis development, and insufficient flow, occur frequently during this remodeling process. These complications can eventually lead to failure and the inability of the fistula to support dialysis. A number of clinical studies have shown that in fistulas that fail to mature the most common anatomical problem is stenosis,[3,16] with intimal hyperplasia (IH) as the underlying cause.[38]

There is general consensus that hemodynamic parameters play an important role in regulating vascular remodeling. Key in this process is the endothelium that senses and responds to significant alterations in wall shear stress (WSS).[10,21,37] Endothelial mechanoreceptors sense the increase in WSS and, through a variety of activated signaling cascades, induce vasodilatation and promote structural changes.[1] Therefore, an investigation of hemodynamics in AVFs, particularly of WSS distribution, and how that relates to vascular remodeling could provide insight into the mechanisms of failure as these mechanisms are still not fully understood.[31]

Developing an understanding of the relationship between vascular remodeling and hemodynamic forces requires accurate measurements of physiological parameters and a detailed 3D analysis of the local blood flow field. Important insights can be obtained by utilizing serial imaging to monitor the evolution of the maturation process over time. The clinical imaging methods that are available have several drawbacks. Digital subtraction angiography (DSA) is the gold standard for angiography as it provides very high spatial resolution, however it is invasive and unsuited to serial 3D monitoring. For blood flow velocity measurements, Doppler ultrasonography (DUS) is limited in its ability to provide a full map of the 3D velocity field. MRI has the unique ability to provide blood flow velocity measurements and 3D angiographic information with anatomical landmarks. This allows straightforward co-registration between time points. A detailed analysis of the local blood flow fields can be obtained in patient-specific geometries using computational fluid dynamic (CFD) models, as demonstrated by numerous studies in intracranial and aortic aneurysms,[28,29] carotid bifurcations, [25,32] and other vascular territories.[36] In AVF investigations, CFD was shown to be a powerful tool for describing flow fields in both idealized models and patient specific geometries.[4,8,15] However, those analyses were performed at single time points, and do not provide a comprehensive correlation of flow factors to the vessel remodeling that is observed in longitudinal studies.

Temporal changes in luminal area, and WSS have been investigated in animal models of graft placement. [26,27] However, very little data describing the changes in humans is available. Description of changes in estimated WSS and vessel diameter at specific locations was obtained by US studies,[5] but no 3D analysis was provided.

The present study aimed to assess the feasibility of using a noncontrast-enhanced MRI protocol combined with CFD modeling to relate hemodynamic changes to vascular remodeling in the 3 months following native AVF placement in humans.

# MATERIALS AND METHODS

## Patient Population

Three male patients (age range: 61–85 years, mean age 76 years) referred to vascular surgery for fistula creation were recruited to this study under IRB approval. Patient demographic data is presented in Table 1. Fistulas in the elbow region were created in all patients as follows: two brachio-cephalic (Patient 1, right arm, and Patient 2, left arm), and one brachiobasilic (Patient 3, left arm). All patients were scanned peri-operatively (within 5 days following surgery), 1 month, and 3 months later.

## MR Imaging

All MR images were obtained on a 1.5T Siemens Avanto scanner (Erlangen Germany) using a surface coil wrapped around the arm at the level of the region of interest. A 2D time of flight (TOF) sequence was used for anastomosis localization. This was followed by a higher resolution 3D TOF acquisition that covered a region of approximately 4 cm above the anastomosis and 2 cm below. The acquisition parameters were as follows: TR/TE = 30/7 ms, flip angle (FA) = 25°, field of view (FOV) = 130 × 113 × 60 $mm^3$, voxel size = 0.25 × 0.25 × 0.6 $mm^3$, receiver bandwidth = 158 Hz/pixel, and number of averages (NA) = 1. Through-plane blood flow velocities in the feeding artery and draining vein were measured 3 cm above the anastomosis. The sagittal and coronal projections (MIP) of the 2D TOF scan were used to position the imaging slice transverse to the vessel of interest. A 2D phase contrast sequence (PC-MRV) was used for the measurements (velocity encoding (VENC) = 150–250 cm/s, TR/TE = 29.5/4.11 ms, FA = 30°, FOV = 200 × 150 $mm^2$, slice thickness = 5 mm, voxel size = 0.78 × 0.78 $mm^2$, receiver bandwidth = 391 Hz/pixel, NA = 3). 20–31 time points were acquired through the cardiac cycle (Fig. 1). Total duration of the study did not exceed 40 min.

## Geometry and Flow Analysis

For each patient, semi-automated segmentation of the 3D TOF data was performed using image analysis software (Amira, Visage Imaging GmbH) to obtain a 3D iso-surface defining the intra-luminal volume of the fistula. Temporal changes in the vascular anatomy were evaluated using this 3D iso-surface. The analysis was performed in Matlab (The MathWorks Inc, Natick, MA). Vascular lumen cross-sections were obtained along the vessel centerline at 0.3 mm intervals, and cross-sectional areas were calculated. The intersection of the centerlines at the anastomosis was used as a landmark. A co-registration of the vascular anatomy was then performed for each patient by applying a rigid transformation (translation and rotation) to each of the lumen cross-sections in order to place them at the corresponding distance from the landmark on the centerline at 3 months post surgery. This method assumes that no changes occurred in the length of the vessels, a fair assumption based on extensive clinical experience in AVF assessment. A direct evaluation of the changes in the length of the vessels was not possible because no landmark points other than the anastomosis could be identified on the TOF-MRA data to enable this analysis.

Analysis of the PC-MRV data was performed offline using Matlab (The MathWorks Inc, Natick, MA). Eddy current induced background phase errors were determined from a linear fit of the static tissue of the arm and subsequently subtracted from the velocity maps.[19] When imaging off-center, strong gradient nonlinearities affect the nominal velocity measurements performed at those locations. Thus, velocity maps were also corrected for gradient field nonlinearity using a method described by Markl *et al.*[24] Briefly, distortion coefficients are calculated from a scanner specific theoretical field model. The coefficients are then used to correct velocity data. Regions of interest (ROI) encompassing the vascular

lumen were drawn by one observer, on the magnitude data and copied to the corrected velocity maps for flow measurements.

### Computational Model

The 3D iso-surface defining the intra-luminal volume of the fistula was transferred into Rapidform (INUS Technology), a 3D modeling software, where a polygonal surface was formed. In order to avoid flow entrance effects, a section of the arterial segment proximal to the anastomosis was included in all CFD models. The computational mesh was generated in Hypermesh (Altair Engineering, Troy, MI) software. An unstructured grid with a nominal resolution of 0.3 mm was generated in all models. This resulted in approximately quarter million cells in each model. For one of the models, a steady flow simulation was conducted on subsequently refined grids. Averaged wall shear stress values computed on a grid with roughly doubled number of cells were within 5% of the values obtained on the original grid. It was therefore decided that the errors due to mesh resolution are sufficiently small and this relatively crude mesh density was used in subsequent analysis, in order to save on computational time in conducting transient simulations for 9 different geometries. Pulsatile flow simulations were carried out at each imaging time point for each patient. A finite-volume package, FLUENT (ANSYS, Inc., Canonsburg, PA) was used to solve the governing Navier–Stokes equations. Time-dependent boundary conditions were prescribed using through-plane PC-MRV measurements over the cardiac cycle. At each computational time step, in addition to specifying the inlet velocity, a targeted flow rate was prescribed at the venous outlet in order to match the flow division between the venous and the distal arterial segments to that measured with MRV. In order to preserve continuity the outlet flow rates were scaled to ensure their sum is equal to the inlet flow rate.

Newtonian flow was assumed in all simulations, with dynamic viscosity of 0.0035 Pa s and density of 1060 kg/m$^3$. Non-Newtonian blood behavior is important when the size of the vessel is comparable to the size of red blood cells, or in regions with low shear stress, which is not the case for the AVF vessels. For this study, intended as an initial investigation, the arterial and venous walls were considered rigid. Second- order schemes were used for numerical discretization in space and time. The iteration steps were repeated until convergence was reached, as indicated by a four order magnitude reduction of the residuals. The unsteady flow simulations were performed through three pulsatile cycles to eliminate the influence of initial transients and results obtained in the last cycle were used for the analysis of the flow fields.

### WSS Analysis

The juxta-anastomotic venous segment (~5 cm) is the region most prone to stenosis development. Therefore, the WSS analysis was focused on this segment. Geometries from the follow-up points were displayed side by side. Two planes were prescribed transverse to the venous segment, one at the level of the suture, and one in the proximal region at the end of the swing segment. The WSS distribution was calculated as a function of covered area in the venous segment contained between the two planes.

## RESULTS

### Temporal Changes of the Vascular Geometry

The angiograms had sufficient image quality to permit vessel segmentation although signal diminution was noted in venous structures as is expected for 3D TOF-MRA. Figure 2 presents a rigid co-registration of the vascular geometries obtained for a brachiocephalic AVF (Patient 1) at 5 days, 1 month, and 3 months after surgery. Note the sharp curvature of the venous segment at 5 days, and the out of plane bends.

The centerline based co-registration is presented in Fig. 3 (left) together with the plots of luminal crosssectional areas of both the vein and the artery, calculated at each time point (right). Arterial luminal cross-sectional areas increased homogeneously along the investigated length. Venous luminal cross-sectional areas showed a more heterogeneous variation along the investigated length. Regions closer to the anastomosis showed a decrease, while regions in the distal vein showed an increase, leading to a greater distribution of sizes at 3 months (Fig. 3). Interestingly, Patient 2 showed a very strong increase in the venous cross-sectional areas at 1 month that was followed by a decrease in most regions at 3 months.

## Temporal Changes of Hemodynamic Parameters

**Flow Visualization—**Flow patterns and WSS distribution for Patient 1 over time are presented in Fig. 4. Streamlines show helical flow in the draining vein at 5 days post surgery that changed into more unidirectional flow at the later time points. Regions of recirculating flow were identified in the vein, at the proximal part of the swing segment at day five, and distal to the anastomosis at 1 and 3 months. Very slow flow was observed in the artery downstream of the anastomosis. Cross-sectional areas in the vein increased with time accompanied by a decrease in blood flow velocities. WSS decreased with time in the entire investigated volume. The WSS profiles also showed a decrease from the anastomosis to the proximal vein [from more red (high WSS) to more blue (low WSS)]. Furthermore, a non-uniform distribution of WSS was observed in the swing segment between the outer and inner walls caused by the high-velocity jet propagating along the outer wall. Higher WSS values were also observed on the outer wall of the proximal part of the swing segment.

Flow patterns and WSS distributions over time for Patient 2 are presented in Fig. 5. Streamlines did not show helical flow in the swing segment at any time point. Regions of recirculating flow were observed in the vein, specifically in the proximal part of the swing segment at day one, in the swing segment at 1 month, and distal to the anastomosis at 3 months. Similar to Patient 1, very slow flow was observed in the artery downstream of the anastomosis at all three time points. Opposite to the uniform increase observed for Patient 1, venous cross-sectional areas in this case showed heterogeneous variation. Narrow regions at 1 day, such as the proximal part of the swing segment, presented a strong increase in vessel diameter; while other regions in the swing segment presented a decrease in diameter at 1 and 3 months. Blood velocities increased during the first month after surgery and subsequently decreased. WSS profiles showed a similar temporal and spatial decrease from the anastomosis to the distal vein as observed for Patient 1. In addition, the heterogeneous distribution of WSS between the outer and inner walls was also observed.

Conversely to the first two patients, with brachiocephalic AVFs, a brachio-basilic AVF was created for Patient 3. Flow patterns and WSS distribution over time are presented in Fig. 6. Streamlines showed helical flow in the vein at all three time points. In addition, blood velocities increased with time. Furthermore, an increase in the cross-sectional area of the anastomosis and the distal vein was observed over time.

The disturbed flow observed in the venous segments resulted in a variability of the WSS distribution and could be responsible for the non-uniform remodeling of the vessel. On the other hand, the artery did not show regions of disturbed flow above the anastomosis, which would be consistent with uniform remodeling.

**Quantitative Analysis—**For each model, the Reynolds numbers based on the diameter and peak systolic velocity at the anastomosis as well as the Womersley numbers are presented in Table 2.

Venous flow was not calculated at the first imaging point for Patient 3 due to aliasing in a very narrow vein. It was estimated as 125% of the arterial flow based on data showing a higher likelihood of retrograde flow in the distal arterial segment, that generally accounts for 25–30% of the venous flow.[33] Furthermore, retrograde flow was actually observed in this patient at one and at 3 months. Flow variation over time for each patient is presented in Table 3. Both arterial and venous flow increased during the first month after surgery in all three patients. Over the following 2 months arterial flow did not show a change for Patients 1 and 3, remaining above 500 mL/min, and decreased for Patient 2. Venous flow remained the same for Patient 1, decreased below 500 mL/min for Patient 2, and increased for Patient 3.

A decrease in mean WSS values of the venous segment from the initial point to 3 months after surgery was observed for Patient 1 (from 31.4 to 9 Pa), and Patient 2 (from 51 to 11 Pa). Conversely, no appreciable change in mean WSS values was observed for Patient 3 (108.4 at 1 day and 110.3 Pa at 3 months). The temporal changes of the WSS distribution in the venous segment as a function of area were calculated for each patient at each time point (Fig. 7).

**Clinical Outcomes—**Long-term clinical follow-up was performed for each patient. By clinical assessment, only one fistula was deemed mature and was used for dialysis at 2 months (Patient 1); at 8 months the patient underwent angioplasty to treat stenosis in the vein. Patient 2 presented with a thrombosed fistula at 10 months but endovascular repair was not attempted because of concern for contrast agent toxicity. No clinical data was available for earlier points. Patient 3 was not started on dialysis because the kidney function was maintained at a level at which dialysis treatment was not necessary. The patient underwent a second stage intervention (venous transposition) after the third MRI study. Subsequently, DSA with balloon angioplasty was performed at 8 months to treat stenoses in the vein, and the fistula eventually failed at 10 months.

## DISCUSSION

Knowledge of the changes in hemodynamic parameters during AVF maturation is expected to improve our understanding of fistula failure, but very little data on actual temporal changes in human AVFs is available in the scientific literature. The present study describes the geometric and hemodynamic changes over time during AVF maturation in humans using MRI/CFD. MRI use demonstrated the ability to provide a comprehensive evaluation of clinically relevant information for the investigation of upper extremity AVFs created in three patients. Using CFD in patient specific geometries, the 3D velocity fields were simulated and WSS was calculated at three different time points during AVF maturation.

AVF maturation is a dynamic process characterized by increase in blood flow rates. The acute pressure drop at the moment of fistula placement produces a tenfold increase in arterial blood flow rate, as measured by duplex Doppler ultrasound. Subsequently, within the first month, a continued strong increase in blood flow is observed, followed by a slower increase at later points.[7,23] The acute change in blood flow rates, from baseline to immediately after fistula placement, was not studied here. However, the changes we observed from immediately after surgery to the later time points (1 and 3 months), are in agreement with previous findings, albeit for fistulas involving the radial artery. At 1 month, blood flow increased in all three fistulas. At 3 months, similar blood flow values compared to the previous point were obtained for two patients and a decrease was found for the third. Because flow rates do not change significantly after 1 month, Robbin *et al.*[30] suggested that blood flow measurements obtained between 4 and 8 weeks can be used to predict fistula outcome, and concluded that an average of 780 ± 401 mL/min relates to successful

maturation and 418 ± 294 mL/min to unsuccessful outcomes. In the present study, arterial blood flow rates at 1 month after surgery were above the average value, predicting a successful outcome. However, only one fistula was considered mature and was used for dialysis, and all three fistulas presented complications after 8 months.

At the moment of fistula placement, in addition to its introduction into the arterial circulation, the venous segment undergoes significant geometrical changes. A segment, called the swing segment, is freed from the surrounding tissue and mobilized toward the artery. This results in ischemia/reperfusion and vessel trauma, possibly damaging the endothelial cell layer. Subsequently, vessel remodeling occurs in three directions: longitudinal, circumferential, and radial.[6] Circumferential remodeling, investigated in our study, was homogeneous in the arterial segment, with low variability of the cross-sectional areas along the length. Conversely, the venous segment presented a heterogeneous remodeling, with high variability of the cross-sectional areas along the investigated segment. The heterogeneous venous remodeling we observed corresponded to disturbed flow patterns in the swing segment, and presence of recirculation regions. Retrospective investigations have shown that stenoses occur predominantly in the swing segment region, specifically at the anastomosis floor, on the inner wall of this segment, and after the curved region (proximal part of the swing segment) when the vein straightens out.[2,34]

Furthermore, the velocity gradients that produce the friction forces sensed by the endothelial cells, are responsible for inducing a variety of activated signaling cascades that result in structural changes in the vessel wall.[1] Understanding the role of the WSS in fistula maturation requires hemodynamic studies during the maturation process itself. CFD modeling is an accurate and comprehensive method that allows characterization of the 3D velocity field and the WSS distribution. [14] A principal result of our study is the description of WSS changes over time in the same patients. Our results are in line with previous CFD investigations of AVFs both in idealized and patient specific models presented at only one time instant.[8,14,15] Flow patterns in the curved regions of the geometry resulted in higher WSS values on the outer curvature and lower WSS on the inner curvature. The low WSS areas corresponded to recirculation regions. Current theories relate stenosis development to these regions of flow recirculation.[9] However, other studies have related high flow rate, rather than low with stenosis development in AVFs.[11,12] It appears from these studies that hemodynamic parameters have an influence on fistula outcome. In addition to these parameters, AVF patency is also linked to the patient's clinical condition and to individual genetic factors involved in the biological responses to injury.[20,22]

## Limitations

Conventional non contrast-enhanced MRA techniques, such as the one used here (TOF), rely on inflow effects and are dependent on blood flow velocities. The variations in blood flow velocities and the asymmetry of the vascular geometry in AVFs may result in spatial variation in magnetization, thus affecting image quality. However, manual segmentation of this data was performed on the source images using a 3 plane viewer, which helped obtain a model as close to the real geometry as possible. We have recently shown that TOF is outperformed by USPIO-enhanced MRA, which provides better luminal delimitation. However, in the same study, diameter measurements correlated well between the two sequences. We can thus assume that the patient specific geometries used were adequate for the purposes of this study. Furthermore, feasibility of non contrast-enhanced MRA has been demonstrated in studies performed on patients with mature failing fistulas, characterized by slow flow.[18,39]

A comparison between baseline and follow-up geometries and flow fields is challenging due to substantial remodeling of the entire venous segment of the AVF. Similarly, correlation

between WSS distribution and the observed vessel remodeling is difficult to obtain. In order to have an objective measure of the changes we used average WSS values over the remodeling venous segment.

We also note that the numerical simulations presented in this study did not account for the vessel wall compliance. The oscillatory motion of the walls due to pulsatile flow could have a noticeable effect on the WSS distribution. This issue will be addressed in future studies by conducting fluid–solid interaction analyses. Also, it is possible that increased flow rates and stenotic constrictions may lead to transitional or turbulent flows in AV fistulas. A critical Reynolds number was estimated for each of the models, based on the formula presented by Stalder *et al.*[35] Comparison of the Reynolds numbers based on the diameter and peak systolic velocity at the anastomosis showed that in all cases the Reynolds numbers did not reach the critical value and the therefore the laminar flow model was likely to be adequate. Additional studies are required to determine whether a laminar solution is sufficiently accurate. Nevertheless, this initial, image-based CFD data elucidates the hemodynamic changes occurring in AV fistulas during maturation.

The specific causes of fistula failure remain unknown. When trying to address this, animal studies are important because of the possibility of performing histological analysis, enabling correlation of hemodynamic findings to the actual structural changes in the vessel wall. A few recent studies have characterized WSS distributions in vascular accesses (grafts and native AVFs) created in animal models and described correlations with vascular remodeling. Two studies used contrast-enhanced MR angiography and 2D PC-MRV to investigate temporal changes in the geometry, flow, and WSS in pigs following placement of PTFE grafts.[26,27] Krishnamoorthy *et al.*[17] applied CFD to simulate complete WSS profiles in two configurations of native AVFs created in pigs. They found an inverse correlation between mean WSS at the time of AVF placement and the degree of luminal stenosis at 42 days post-surgery.

## CONCLUSION

MRI is the most suitable modality for studying the maturation of AV fistulas, as it provides an angiographic map, velocity measurements, and, potentially, information on the vessel wall morphology, all in one imaging session. 3D geometry offers a complete view of fistula evolution over time, and in combination with MR velocity data, provides the opportunity to perform detailed CFD analysis of local hemodynamics in order to determine flow descriptors affecting fistula maturation.

## Acknowledgments

This work has been supported by a VA Merit award (DS), and a NIH grant NS059891 (VR).

## References

1. Achneck HE, Sileshi B, Li M, Partington EJ, Peterson DA, Lawson JH. Surgical aspects and biological considerations of arteriovenous fistula placement. Semin Dial. 2010; 23:25–33. [PubMed: 20331815]
2. Badero OJ, Salifu MO, Wasse H, Work J. Frequency of swing-segment stenosis in referred dialysis patients with angiographically documented lesions. Am J Kidney Dis. 2008; 51:93–98. [PubMed: 18155537]
3. Beathard GA, Arnold P, Jackson J, Litchfield T. Aggressive treatment of early fistula failure. Kidney Int. 2003; 64:1487–1494. [PubMed: 12969170]

4. Carroll GT, McGloughlin TM, Burke PE, Egan M, Wallis F, Walsh MT. Wall shear stresses remain elevated in mature arteriovenous fistulas: a case study. J Biomech Eng. 2011; 133:021003. [PubMed: 21280875]
5. Dammers R, Tordoir JH, Kooman JP, Welten RJ, Hameleers JM, Kitslaar PJ, Hoeks AP. The effect of flow changes on the arterial system proximal to an arteriovenous fistula for hemodialysis. Ultrasound Med Biol. 2005; 31:1327–1333. [PubMed: 16223635]
6. Dixon BS. Why don't fistulas mature? Kidney Int. 2006; 70:1413–1422. [PubMed: 16883317]
7. Ene-Iordache B, Mosconi L, Antiga L, Bruno S, Anghileri A, Remuzzi G, Remuzzi A. Radial artery remodeling in response to shear stress increase within arteriovenous fistula for hemodialysis access. Endothelium. 2003; 10:95–102. [PubMed: 12791517]
8. Ene-Iordache B, Mosconi L, Remuzzi G, Remuzzi A. Computational fluid dynamics of a vascular access case for hemodialysis. J Biomech Eng. 2001; 123:284–292. [PubMed: 11476373]
9. Ene-Iordache B, Remuzzi A. Disturbed flow in radial-cephalic arteriovenous fistulae for haemodialysis: low and oscillating shear stress locates the sites of stenosis. Nephrol Dial Transplant. 2011; 27:358–368. [PubMed: 21771751]
10. Helmke BP, Davies PF. The cytoskeleton under external fluid mechanical forces: hemodynamic forces acting on the endothelium. Ann Biomed Eng. 2002; 30:284–296. [PubMed: 12051614]
11. Hofstra L, Bergmans DC, Leunissen KM, Hoeks AP, Kitslaar PJ, Daemen MJ, Tordoir JH. Anastomotic intimal hyperplasia in prosthetic arteriovenous fistulas for hemodialysis is associated with initial high flow velocity and not with mismatch in elastic properties. J Am Soc Nephrol. 1995; 6:1625–1633. [PubMed: 8749690]
12. Hofstra L, Bergmans DC, Leunissen KM, Hoeks AP, Kitslaar PJ, Tordoir JH. Prosthetic arteriovenous fistulas and venous anastomotic stenosis: influence of a high flow velocity on the development of intimal hyperplasia. Blood Purif. 1996; 14:345–349. [PubMed: 8894129]
13. III. NKF-K/DOQI clinical practice guidelines for vascular access: Update 2000. Am J Kidney Dis. 2001; 37:S137–S181. [PubMed: 11229969]
14. Kharboutly Z, Deplano V, Bertrand E, Legallais C. Numerical and experimental study of blood flow through a patient-specific arteriovenous fistula used for hemodialysis. Med Eng Phys. 2010; 32:111–118. [PubMed: 19962337]
15. Kharboutly Z, Treutenaere JM, Claude I, Legallais C. Arterio-venous fistula: two cases realistic numerical blood flow simulations. Conf Proc IEEE Eng Med Biol Soc. 2007; 2007:2980–2983. [PubMed: 18002621]
16. Kheda MF, Brenner LE, Patel MJ, Wynn JJ, White JJ, Prisant LM, Jones SA, Paulson WD. Influence of arterial elasticity and vessel dilatation on arteriovenous fistula maturation: a prospective cohort study. Nephrol Dial Transplant. 2010; 25:525–531. [PubMed: 19755475]
17. Krishnamoorthy MK, Banerjee RK, Wang Y, Zhang J, Roy AS, Khoury SF, Arend LJ, Rudich S, Roy-Chaudhury P. Hemodynamic wall shear stress profiles influence the magnitude and pattern of stenosis in a pig AV fistula. Kidney Int. 2008; 74:1410–1419. [PubMed: 18818686]
18. Laissy JP, Menegazzo D, Debray MP, Loshkajian A, Viron B, Mignon F, Schouman-Claeys E. Failing arteriovenous hemodialysis fistulas: assessment with magnetic resonance angiography. Invest Radiol. 1999; 34:218–224. [PubMed: 10084667]
19. Lankhaar JW, Hofman MB, Marcus JT, Zwanenburg JJ, Faes TJ, Vonk-Noordegraaf A. Correction of phase offset errors in main pulmonary artery flow quantification. J Magn Reson Imaging. 2005; 22:73–79. [PubMed: 15971181]
20. Lazo-Langner A, Knoll GA, Wells PS, Carson N, Rodger MA. The risk of dialysis access thrombosis is related to the transforming growth factor-beta1 production haplotype and is modified by polymorphisms in the plasminogen activator inhibitor-type 1 gene. Blood. 2006; 108:4052–4058. [PubMed: 16931622]
21. Lehoux S, Tedgui A. Signal transduction of mechanical stresses in the vascular wall. Hypertension. 1998; 32:338–345. [PubMed: 9719064]
22. Lin CC, Yang WC, Lin SJ, Chen TW, Lee WS, Chang CF, Lee PC, Lee SD, Su TS, Fann CS, Chung MY. Length polymorphism in heme oxygenase-1 is associated with arteriovenous fistula patency in hemodialysis patients. Kidney Int. 2006; 69:165–172. [PubMed: 16374439]

23. Lomonte C, Casucci F, Antonelli M, Giammaria B, Losurdo N, Marchio G, Basile C. Is there a place for duplex screening of the brachial artery in the maturation of arteriovenous fistulas? Semin Dial. 2005; 18:243–246. [PubMed: 15934972]
24. Markl M, Bammer R, Alley MT, Elkins CJ, Draney MT, Barnett A, Moseley ME, Glover GH, Pelc NJ. Generalized reconstruction of phase contrast MRI: analysis and correction of the effect of gradient field distortions. Magn Reson Med. 2003; 50:791–801. [PubMed: 14523966]
25. Milner JS, Moore JA, Rutt BK, Steinman DA. Hemodynamics of human carotid artery bifurcations: computational studies with models reconstructed from magnetic resonance imaging of normal subjects. J Vasc Surg. 1998; 28:143–156. [PubMed: 9685141]
26. Misra S, Fu AA, Misra KD, Glockner JF, Mukhopadhyay D. Wall shear stress measurement using phase contrast magnetic resonance imaging with phase contrast magnetic resonance angiography in arteriovenous polytetrafluoroethylene grafts. Angiology. 2009; 60:441–447. [PubMed: 19625275]
27. Misra S, Woodrum DA, Homburger J, Elkouri S, Mandrekar JN, Barocas V, Glockner JF, Rajan DK, Mukhopadhyay D. Assessment of wall shear stress changes in arteries and veins of arteriovenous polytetrafluoroethylene grafts using magnetic resonance imaging. Cardiovasc Intervent Radiol. 2006; 29:624–629. [PubMed: 16729233]
28. Rayz VL, Boussel L, Acevedo-Bolton G, Martin AJ, Young WL, Lawton MT, Higashida R, Saloner D. Numerical simulations of flow in cerebral aneurysms: comparison of CFD results and in vivo MRI measurements. J Biomech Eng. 2008; 130:051011. [PubMed: 19045518]
29. Rayz VL, Boussel L, Lawton MT, Acevedo-Bolton G, Ge L, Young WL, Higashida RT, Saloner D. Numerical modeling of the flow in intracranial aneurysms: prediction of regions prone to thrombus formation. Ann Biomed Eng. 2008; 36:1793–1804. [PubMed: 18787954]
30. Robbin ML, Chamberlain NE, Lockhart ME, Gallichio MH, Young CJ, Deierhoi MH, Allon M. Hemodialysis arteriovenous fistula maturity: US evaluation. Radiology. 2002; 225:59–64. [PubMed: 12354984]
31. Roy-Chaudhury P V, Sukhatme P, Cheung AK. Hemodialysis vascular access dysfunction: a cellular and molecular viewpoint. J Am Soc Nephrol. 2006; 17:1112–1127. [PubMed: 16565259]
32. Schirmer CM, Malek AM. Patient based computational fluid dynamic characterization of carotid bifurcation stenosis before and after endovascular revascularization. J Neurointerv Surg. 2011; 4(6):448–454. [PubMed: 22039041]
33. Sivanesan S, How TV, Bakran A. Characterizing flow distributions in AV fistulae for haemodialysis access. Nephrol Dial Transplant. 1998; 13:3108–3110. [PubMed: 9870474]
34. Sivanesan S, How TV, Bakran A. Sites of stenosis in AV fistulae for haemodialysis access. Nephrol Dial Transplant. 1999; 14:118–120. [PubMed: 10052489]
35. Stadler, AF.; Frydrychowich, A.; Russe, MF.; Korvink, JG.; Hennig, J.; Li, KC.; Markl, M. Analysis of Reynolds, Strouhal and Womerseley numbers in the healthy thoracic aorta. Proceedings of the International Society for Magnetic Resonance in Medicine; 2011.
36. Suh GY, Les AS, Tenforde AS, Shadden SC, Spilker RL, Yeung JJ, Cheng CP, Herfkens RJ, Dalman RL, Taylor CA. Hemodynamic changes quantified in abdominal aortic aneurysms with increasing exercise intensity using MR exercise imaging and imagebased computational fluid dynamics. Ann Biomed Eng. 2011; 39:2186–2202. [PubMed: 21509633]
37. Traub O, Berk BC. Laminar shear stress: mechanisms by which endothelial cells transduce an atheroprotective force. Arterioscler Thromb Vasc Biol. 1998; 18:677–685. [PubMed: 9598824]
38. Van Tricht I, De Wachter D, Tordoir J, Verdonck P. Hemodynamics and complications encountered with arteriovenous fistulas and grafts as vascular access for hemodialysis: a review. Ann Biomed Eng. 2005; 33:1142–1157. [PubMed: 16175669]
39. Waldman GJ, Pattynama PM, Chang PC, Verburgh C, Reiber JH, de Roos A. Magnetic resonance angiography of dialysis access shunts: initial results. Magn Reson Imaging. 1996; 14:197–200. [PubMed: 8847975]

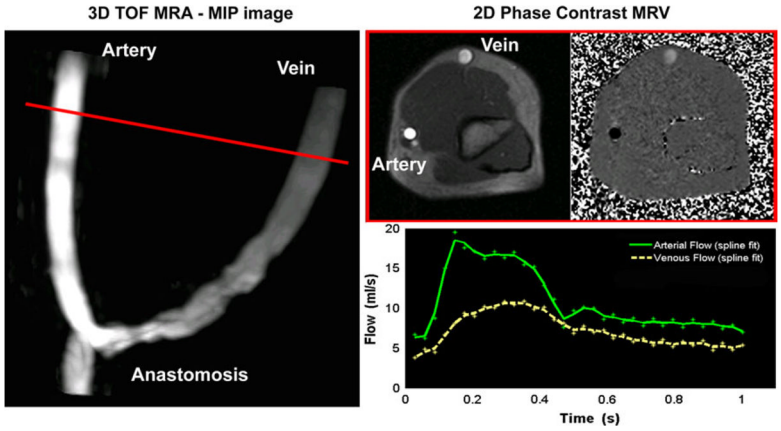


**FIGURE 1.**

MR images acquired at 3 months after surgery for Patient 2. Left: full thickness MIP image of the brachio-cephalic fistula, and the approximate location of the imaging plane used for velocity measurements. Right: magnitude and phase 2D PCMRV images (Top), time resolved volumetric flowrate waveforms measured in the brachial artery and in the cephalic vein (Bottom).

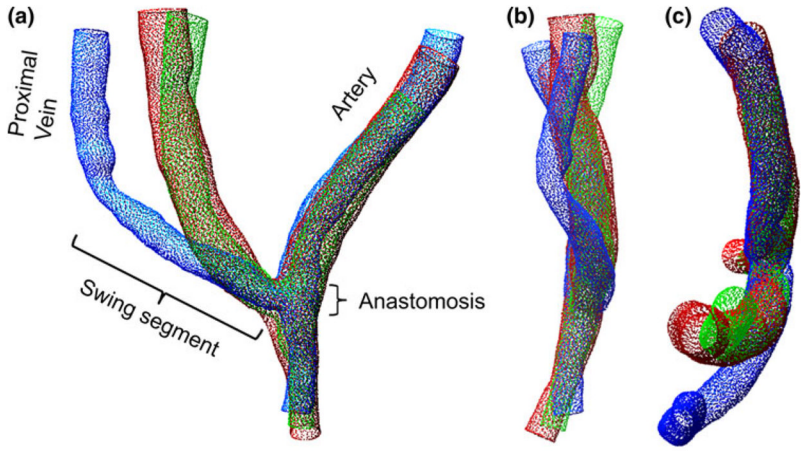


**FIGURE 2.**

Rigid co-registration of vascular geometries from 5 days (blue), 1 month (green) and 3 months (red) after placement of a brachio-cephalic fistula for Patient 1. Lateral (a), side (b) and top (c) views. Note the sharp curvature of the venous segment, particularly at 5 days (a), and the out of plane bend (b).

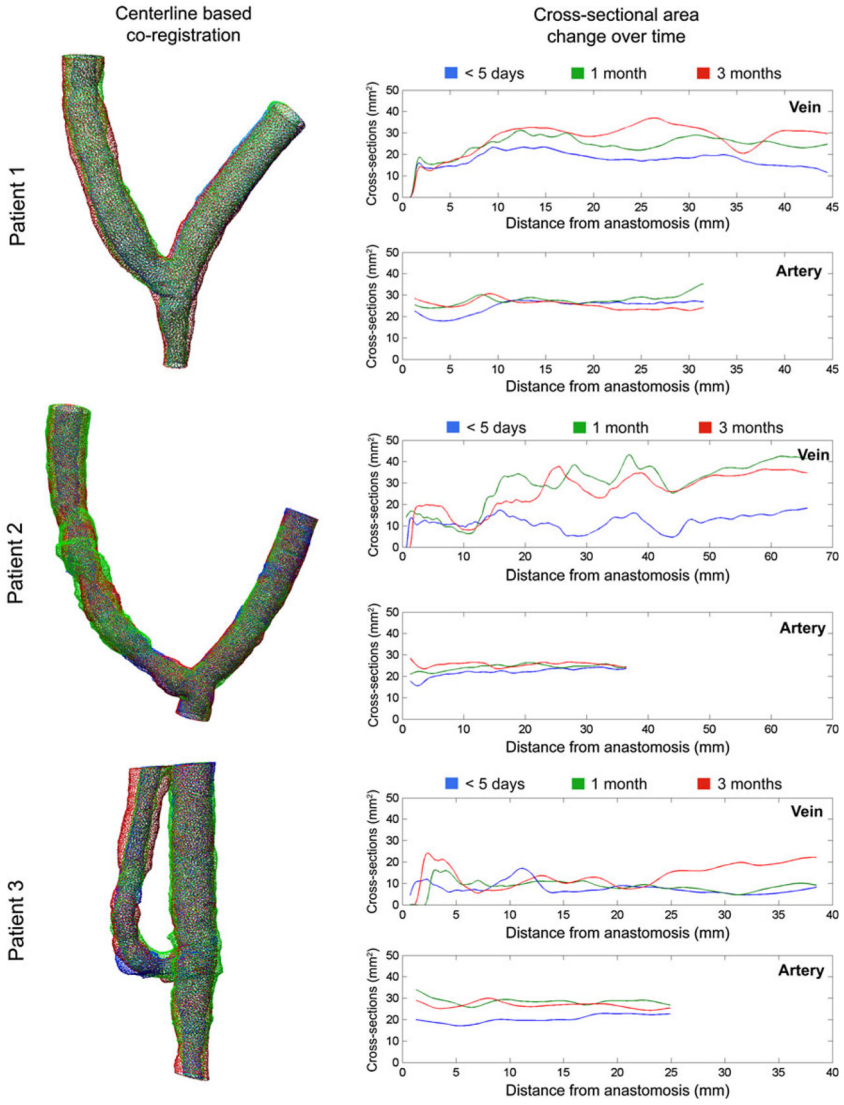


**FIGURE 3.**

Center-line based co-registration of luminal geometries for Patient 1, Patient 2, and Patient 3 (left). Venous and arterial cross-sectional area change over time (right). Note the strong increase in cross-sectional area in several regions of the vein at 1 month post surgery for Patient 2 followed by a decrease at 3 months.

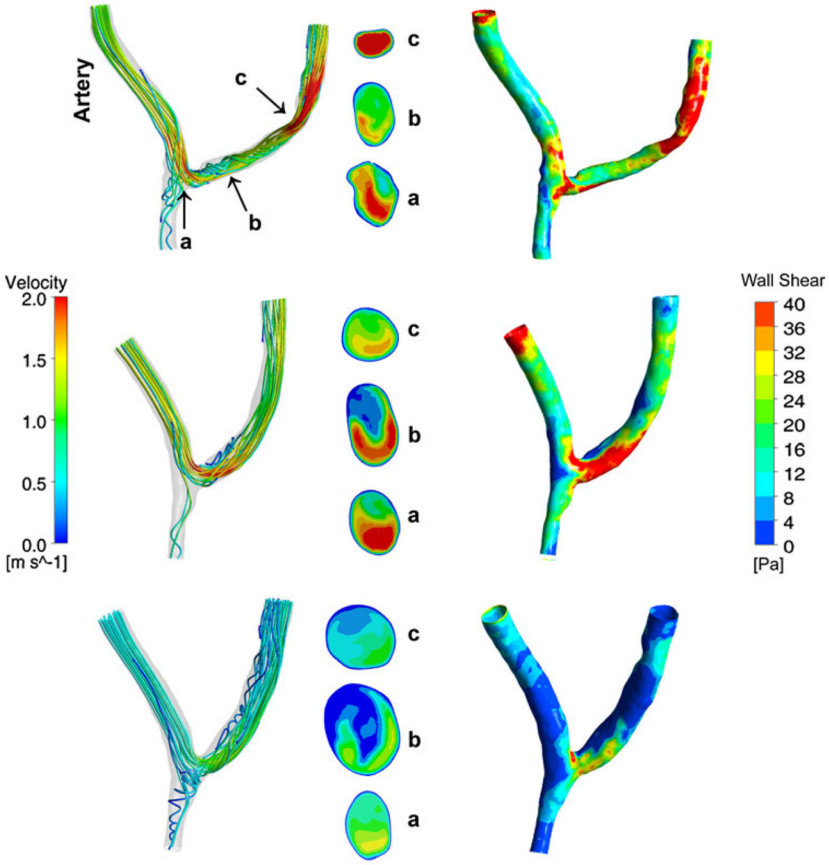


**FIGURE 4.**

Comparison of the velocity fields (left) and WSS distributions (right) in a patient specific geometry of a brachiocephalic AVF (Patient 1) from top to bottom: at 5 days, 1 month and 3 months following fistula placement surgery. Cross-sectional images at each time point present the velocity magnitude at the anastomosis (a), in the swing segment (b), and the proximal part of the swing segment (c).

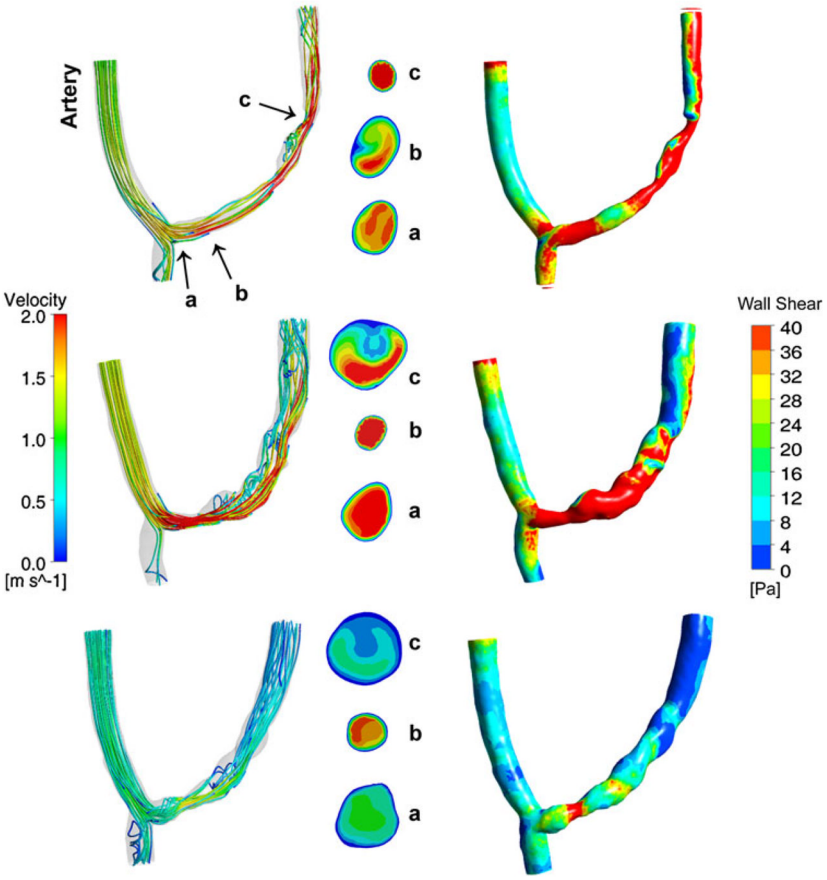


**FIGURE 5.**

Comparison of the velocity fields (left) and WSS distributions (right) in a patient specific geometry of a brachiocephalic AVF (Patient 2) from top to bottom: at 1 day, 1 month and 3 months following fistula placement surgery. Cross-sectional images at each time point present the velocity magnitude at the anastomosis (a), in the swing segment (b), and the proximal part of the swing segment (c).

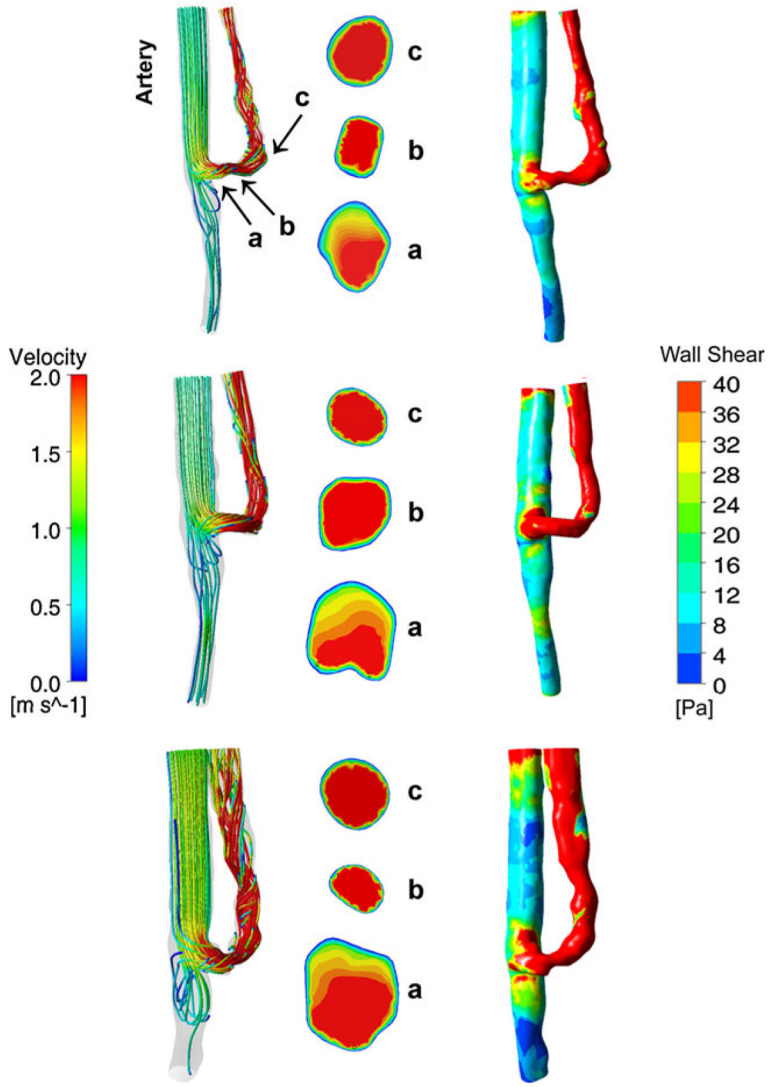


**FIGURE 6.**

Comparison of the velocity fields (left) and WSS distributions (right) in a patient specific geometry of a brachio-basilic AVF (Patient 3) from top to bottom: at 1 day, 1 month and 3 months following fistula placement surgery. Cross-sectional images at each time point present the velocity magnitude at the anastomosis (a), in the swing segment (b), and the proximal part of the swing segment (c).

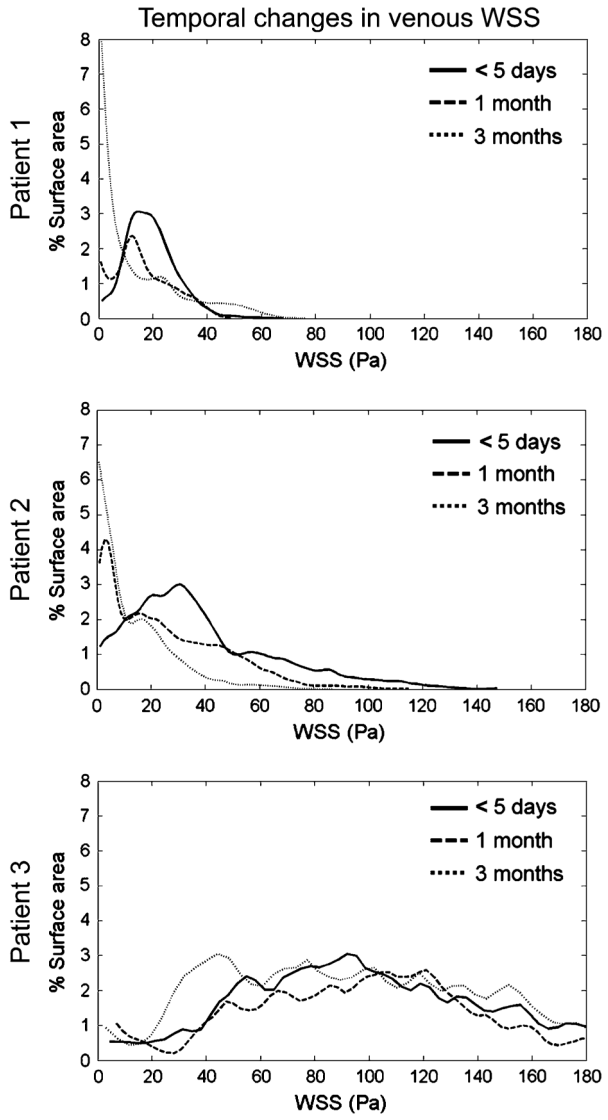


**FIGURE 7.**

Plots showing the distribution of WSS values obtained at peak systole in the venous segment at each time point. Note that WSS values decrease with time for Patients 1 and 2, and remain relatively unchanged for Patient 3.

## TABLE 1

Patient demographic data ($n = 3$).

| Characteristic | Number |
|---|---|
| Age, average (range) | 76 (61–85) |
| Male sex | 3/3 |
| Race | |
| White | 1/3 |
| Black | 2/3 |
| Hypertension | 3/3 |
| Coronary artery disease (CAD) | 1/3 |
| Diabetes mellitus (DM) | 1/3 |
| Hyperlipidemia | 2/3 |
| On dialysis at study enrollment | 2/3 |
| eGFR if not on dialysis, average ml/min/1.73 $m^2$ | 13 |
| Causes of renal failure | |
| Ischemic nephropathy | 1/3 |
| Diabetes and hypertension | 1/3 |
| Hypertension | 1/3 |

## TABLE 2

Reynolds number based on the diameter and peak systolic velocity at the anastomosis, and Womersley number for each patient and the three follow-up points.

| | Reynolds number (anastomosis) | Womersley number |
|---|---|---|
| Patient 1 | | |
| Point 1 | 1274 | 3.97 |
| Point 2 | 1359 | 3.43 |
| Point 3 | 969 | 3.64 |
| Patient 2 | | |
| Point 1 | 1314 | 2.57 |
| Point 2 | 1899 | 3.29 |
| Point 3 | 834 | 3.46 |
| Patient 3 | | |
| Point 1 | – | 2.75 |
| Point 2 | 1599 | 2.81 |
| Point 3 | 2130 | 3.39 |

## TABLE 3

Temporal variation of the volume flow in both the artery and the vein.

| | <5 days | 1 month | 3 months |
|---|---|---|---|
| Patient 1 | | | |
| Artery | 520 | 906 | 814 |
| Vein | 513 | 718 | 700 |
| Patient 2 | | | |
| Artery | 1078.5 | 1217 | 658 |
| Vein | 776 | 971 | 430 |
| Patient 3 | | | |
| Artery | 436 | 1104 | 1180 |
| Vein | – | 1160 | 1363 |